Numerical Simulation Study for the Structure and Evolution of Tropical Squall Line①

Sun Tingkai (孙廷凯) and Tan Zhemin (谈哲敏)

Key Laboratory for Meso-scale Severe Weather/ MOE, Department of Atmospheric Sciences, Nanjing University, Nanjing 210093

P44 A

(Received January 20, 2000; revised August 15, 2000)

ABSTRACT

The occurrence and evolution of an oceanic tropical squall line observed on 22 February 1993 during TOGA-COARE over the equatorial Pacific Ocean were simulated by use of a three-dimensional, nonhydrostatic storm-scale numerical model ARPS. The capacity of ARPS to simulate such tropical squall line was verified. The structure and dynamic mechanism of the squall line were discussed in details as well. The impacts of the different microphysical process that including the ice phase and warm rain schemes on structure and evolution of the squall line were investigated by the sensitive experiment.

The simulations of the three-dimensional structure and evolution of the squall line are closely related with the observations when the proper microphysical processes were employed. The more latent heating released in the ice phase processes associated with the freezing process leads to strengthening deep convection due to the vertical gradient of buoyancy, which results in a long life of the convective system. In contrast, the warm rain process is characterized by short life period, more pronounced rearward tilt structure and extension of stratiform cloud.

Key words: Squall line, Cold pool, Ice phase microphysics, Cloud-resolving model

1. Introduction

Mesoscale convection system (MCS) could be regarded as a primary unit of energy transportation in the vertical and has an important role in the large-scale motion (Houze, 1982). However, so far the deep convection system could not be resolvable or simulated explicitly in global circulation models (GCM) due to the limiting of calculation condition and the lacking of sufficient physical understanding. Therefore, the parameterization methods for the sub-grid scale processes have to be employed in GCM. GCSS (GEWEX Cloud System Study) is a subprogram of GEWEX (Global Energy and Water Cycle Experiment). The main objective of GCSS is the improving of the parameterization of cloud related processes in general circulation and numerical weather predication models through the improved physical understanding of these processes (Moncrieff et al., 1997). The main tool of GCSS is the cloud-resolving model (CRM) which is a numerical model that resolves cloud-scale (and mesoscale) circulation in either two or three spatial dimensions. Therefore, further research on the physical mechanism of convective system will benefit to the improvement of cumulus

①This research was supported by the National Natural Science Foundation of China under the grant Nos. 49605064 and 49735180, and by State Key Basic Research Program: Research on the Formation Mechanism and Predication Theory of Hazardous Weather over China (CHERES, No. G1998040907).

convection parameterization in GCM.

In tropical region, the severe convection system is one of the most important mesoscale systems. It plays a crucial role in transportation of momentum, heat and kinetic energy therefore results in effect on the large scale circulation. The interactions between MCS and large-scale circulation in tropical region have significant impacts on the atmosphere-ocean interaction and the tropical climate change. The one of purpose of the Tropical Ocean Global Atmosphere (TOGA) Coupled Ocean-Atmosphere Response Experiment (COARE) conducted from November 1992 to March 1993 is to study the occurrence of MCS in the western Pacific Ocean warm pool region and the effects on tropical large-scale atmospheric circulation (Webster and Lukas, 1992). During the intensive observation period (IOP) of TOGA-COARE, Doppler radars, airplanes and other instruments were used to observe the MCS occurrence intensively during this period. Rickenbach and Rutledge (1998) analyzed the shipboard radar IOP data of TOGA-COARE and found that 75% of total precipitation cases are relevant to MCS and nearly 50% of all linear convective organizations have characteristics of tropical squall line. During the period after the appearance of an oceanic squall line, a tropical cyclone may be emerged from just the same region (Jorgensen et al., 1997).

In general, the squall lines are characterized by the low-level jet. The low-level vertical wind shear is perpendicular to the leading edge of convection and the system moves forwards at the speed of low-level jet. The updraft tilt structure of squall line is determined primarily by the interaction between the subcloud cold pool internally generated and the low-level vertical environmental wind shear (Rotunno et al., 1988). The vertical vorticity in the squall line system is generated not only from the tilting of environment horizontal vorticity, but also from the vertical wind shear induced by horizontal gradient of buoyancy. However, the horizontal gradient of buoyancy is closely related to the low-level cold pool and water loading (Trier et al., 1997). Therefore, the structure of low-level cold pool and the distribution of water material, which are closely related to cloud microphysical processes, are crucial in the simulation of squall line.

Though the evolution and structure of squall line mainly depend on the large-scale environmental flow, the cloud microphysical process is also a crucial factor that could affect the internal dynamics processes of squall line. The ice phase processes could affect the height of convection and the developments of stratiform clouds rearward of squall line (Tao and Simpson, 1989). Furthermore, the cloud microphysical processes could affect the structure of cold pool near the leading edge and the propagation speed of squall line. Also the updraft tilt structure and the distribution of water material could be affected further (Ferrier et al., 1995).

Trier et al. (1996) simulated the squall line occurred on 22 February 1993 during the period of TOGA-COARE by a cloud model. The impacts of surface flux and cloud microphysical processes on the structures of updraft tilt and cold pool are investigated. The effect of surface flux induced internally on evolution of squall line was solely investigated in their study, however, the detail analysis of dynamic and thermal structure, and the evolution processes of some related physical variables were ignored. The GCSS Working Group 4 (WG4, Precipitating Convective Cloud System) completed the comparison of eight cloud-resolving models for this tropical squall line case (Redelsperger et al., 2000).

In the current study, a three-dimensional, nonhydrostatic and storm-scale numerical model ARPS (Xue et al., 1995) is adopted to simulate the generation and evolution of a tropical squall line observed on 22 February 1993 during the Intensive Observation Period

of TOGA COARE. The structure and behavior ofthe squall line, and the time-dependent features of some related variables are investigated to verify the capability of ARPS. Moreover, the impacts of different cloud microphysical processes on the structure and evolution of the squall line were discussed.

Section 2 provides the experimental design and initial conditions. The simulation and analysis for the structure and evolution of the squall line are shown in Section 3. In Section 4, the effects of different cloud microphysical processes on structure and behavior of squall line are discussed. The summary and conclusion are given in Section 5.

2. Experimental design

In this study, we will adopt the Advanced Regional Predication System (ARPS, see Xue et al., 1995) for numerical simulation. ARPS is a three-dimensional, nonhydrostatic, compressible and storm-scale numerical model. In our study it is a horizontal domain of 103 × 103 grids with horizontal resolution of 1.25 km. It has 33 levels from bottom to the model top with a vertically stretched grid in which Δz is about 100 m below 8 km and then becomes about 700 m above 8 km. The actual domain is $125 \times 125 \times 15$ km^3. In order to keep the squall line inside the simulation domain, the model domain is translated along with the squall line. Open lateral boundary condition is used. The upper and bottom boundaries are rigid. Sponge damped level is adopted above 12 km to reduce the reflection of gravitational wave. 1.5 order TKE closure scheme is adopted for the sub-grid scale turbulence. For simplicity, rotation effects (Coriolis force) are ignored.

The model is initialized by a single sounding at all model grid points. The convection is initiated by a line of three 1 km-deep cold columns of 5 km radius and −8K temperature deficit. They are south-to-north oriented with the interval of 2.5 km. Fig. 1 shows the initial sounding data. From Fig. 1a, we can infer that the CAPE for irreversible pseudo-adiabatic ascent of an air package at the lowest 50 hPa is about 1500 J / kg. Fig. 1b shows that there is a strong vertical wind shear in the lowest 2 km and the axis of low-level jet is about 2 km high. Above the axis, there is a weak wind upshear.

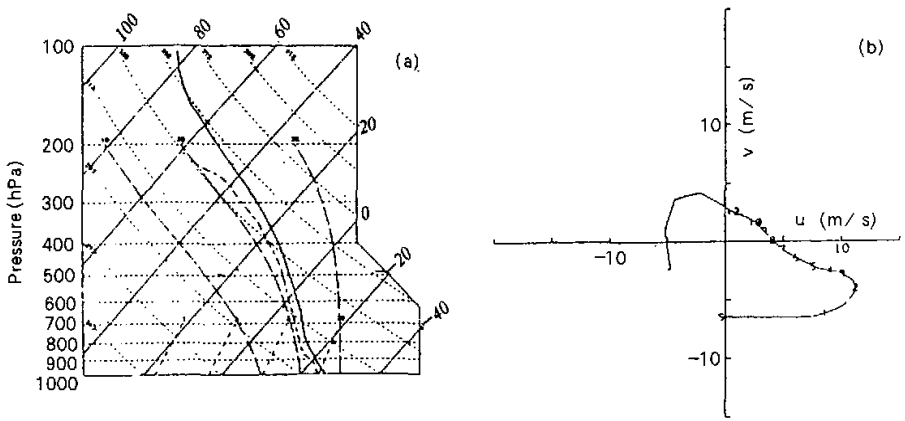

Fig. 1 (a). Initial temperature (solid line) and dewpoint (dashed line) curves in °C; and (b) initial hodograph (m / s) for numerical simulation (after Trier et al., 1996).

In this study, two experiments are designed. One is control experiment (CRTL) in which the ice phase microphysical process is adopted that including the water vapor (q_v), cloud water (q_c), rain water (q_r), cloud ice (q_i), snow (q_s) and cloud hail (q_h). The other is the warm rain experiment (WARM) in which the Kessler warm rain scheme is adopted that including the water vapor (q_v), cloud water (q_c) and rain water (q_r).

3. Results

3.1 *Midlevel structure of squall line*

In general, the squall line appears as a narrow convection band below the height of 5 km, however, as a convective cloud cluster above this height. At the low–level, the convection line band is narrowest and weak. Therefore, in this section we focus on the structure and evolution of the squall line at the midlevel. Figs. 2a, 2b, 2c and 2d show the midlevel structure of squall line for CRTL at the $t=3$, 3.5, 4 and 5 hour, respectively. Triggered by the initial temperature perturbation, the local subsidence nearby three cold columns begins to accumulate cold air on the surface. The warm air between cold columns is crushed and forced to rise, consequently three local ascent centers appeared, accompanied by some weak sinking regions around. At $t=2$ hour, the convective cells seemed to buildup a relatively independent convective line.

The squall line grew into a linear bow–shaped strong convective system at $t=3$ hour. Fig. 2a revealed that the convection region was constituted by many convective cells and was stronger than before. The maximal updraft velocity was about 7.79 ms^{-1}. The intensity and range of sinking motion rearward the leading edge of squall line (namely leading line thereafter) are increased. The leading line represents itself as a convergent draft region in horizontal wind field. Subsequently the squall line increased in convective intensity and horizontal scale. The maximal vertical velocity is about 9.08 ms^{-1} at $t=3.5$ hour (Fig. 2b). Near the northern segment, the flows coming from north and both laterals of leading line assembled behind it. Near the middle segment the fore inflow and rear inflow assembled behind the leading line and a relatively weak cyclone was formed rear it. Near the southern part the fore inflow and northward flow assembled behind the leading line and a relative strong anticyclone was generated.

By 4 h into the simulation, the updraft motion is increased continuously (Fig. 2c). The maximal upward velocity is about 9.59 ms^{-1} and the maximal downward velocity is about 2.2 ms^{-1}. Moreover, the new convective cells were formed rear to the southern portion. At $t=5$ h, the convective system comes into a period of attenuation (Fig. 2d). The squall line increased in horizontal scale but decreased in convective intensity, and became an unorganized band consisted of many discrete convective cells. Many disperse subsidence regions appeared the rearward of the leading line. The squall line changes from bow–shaped structure to quasi–two dimensional one that will be kept until the convection region dissipated.

3.2 *The dynamic and thermal vertical structure of squall line*

In Section 3.1, we know that during the period from 3 h to 4 h, the convection increased obviously. During this period, the updraft tilt is enhanced, and the stratiform cloud precipitation is increased. In this subsection, the vertical cross–sections of the vertical motion and water material at the middle segment are presented to reflect some general characters of convection line.

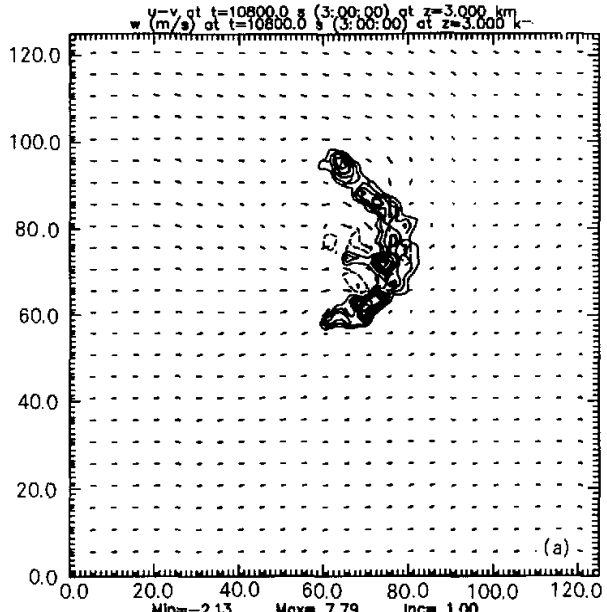
v-v at t=10800.0 s (3:00:00) at z=3.000 km
w (m/s) at t=10800.0 s (3:00:00) at z=3.000 k
120.0
100.0
80.0
60.0
40.0
20.0
0.0
0.0 20.0 40.0 60.0 80.0 100.0 120.0
(a)
Min=-2.13 Max= 7.79 Inc= 1.00
dL_s.o Umin= -4.40 Umax= 5.75 Vmin= -6.47 Vmax= 3.62

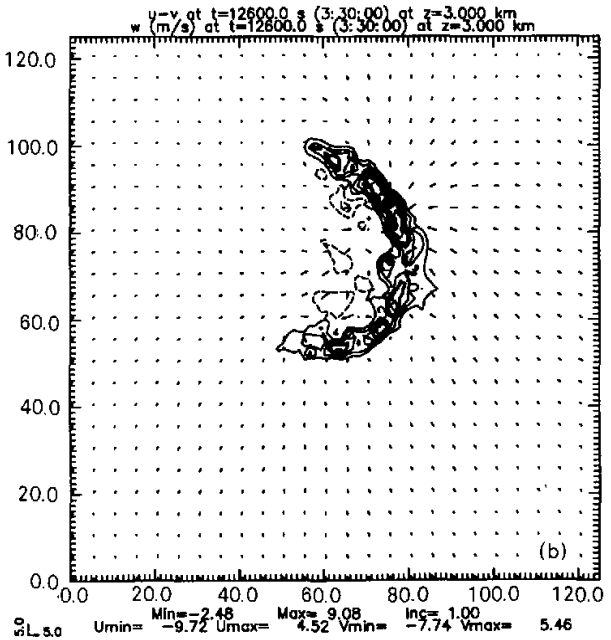
v-v at t=12600.0 s (3:30:00) at z=3.000 km
w (m/s) at t=12600.0 s (3:30:00) at z=3.000 km
120.0
100.0
80.0
60.0
40.0
20.0
0.0
0.0 20.0 40.0 60.0 80.0 100.0 120.0
(b)
Min=-2.48 Max= 9.08 Inc= 1.00
dL_s.o Umin= -9.72 Umax= 4.52 Vmin= -7.74 Vmax= 5.46

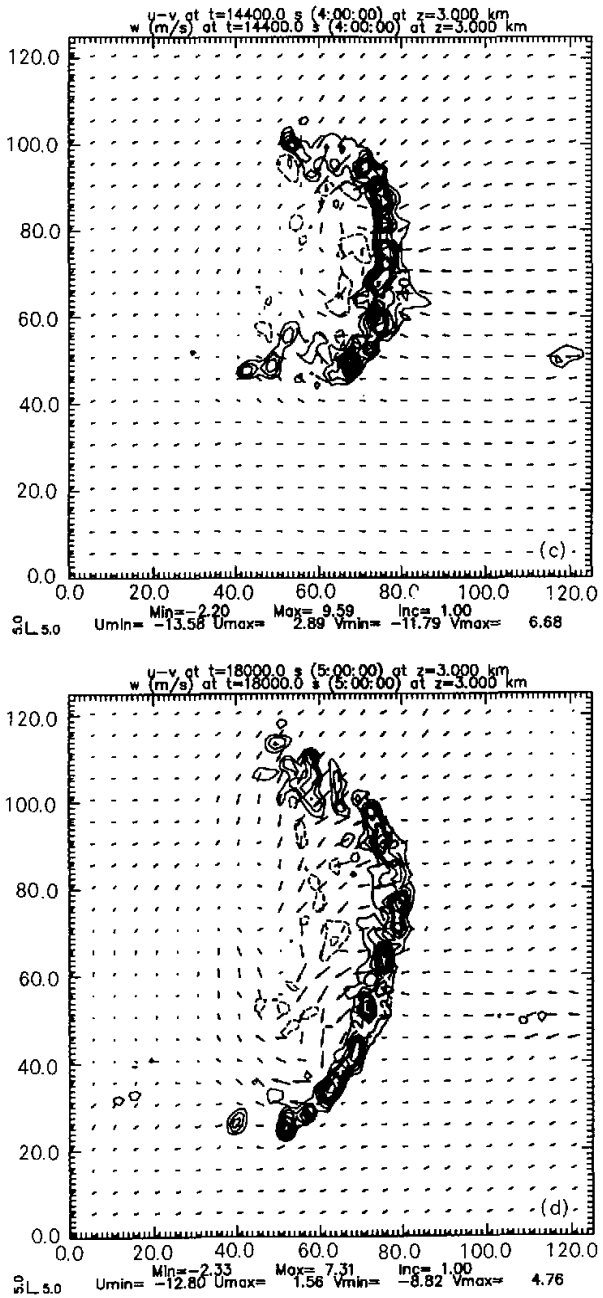

Fig. 2. Vertical velocity at 3 km MSL in intervals of 1 m/s (positive values solid, negative values dashed) and system-relative wind vectors at 3 km MSL for CRTL at (a) 3 h, (b) 3.5 h, (c) 4 h, and (d) 5 h.

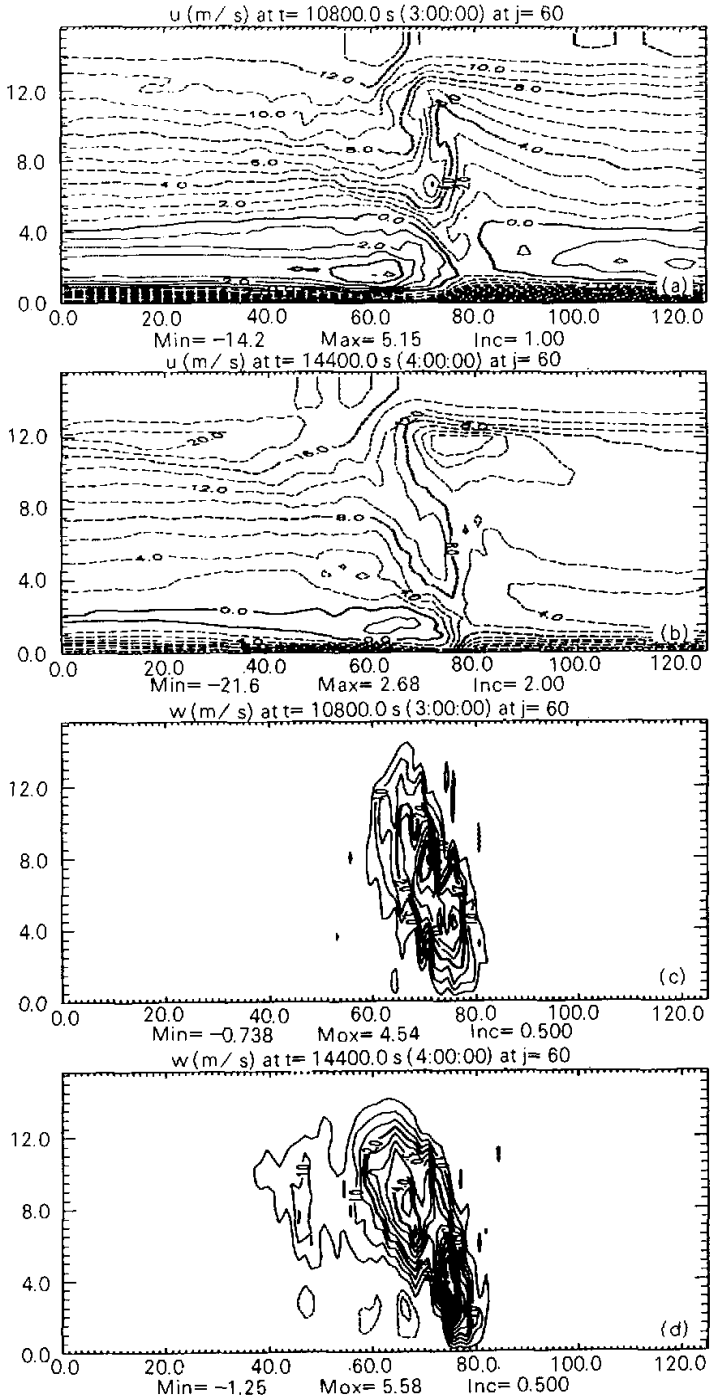
u (m/ s) at t= 10800.0 s (3:00:00) at j= 60
Min= −14.2 Max= 5.15 Inc= 1.00
(a)
u (m/ s) at t= 14400.0 s (4:00:00) at j= 60
Min= −21.6 Max= 2.68 Inc= 2.00
(b)
w (m/ s) at t= 10800.0 s (3:00:00) at j= 60
Min= −0.738 Max= 4.54 Inc= 0.500
(c)
w (m/ s) at t= 14400.0 s (4:00:00) at j= 60
Min= −1.25 Max= 5.58 Inc= 0.500
(d)
0.0 4.0 8.0 12.0
0.0 20.0 40.0 60.0 80.0 100.0 120.0

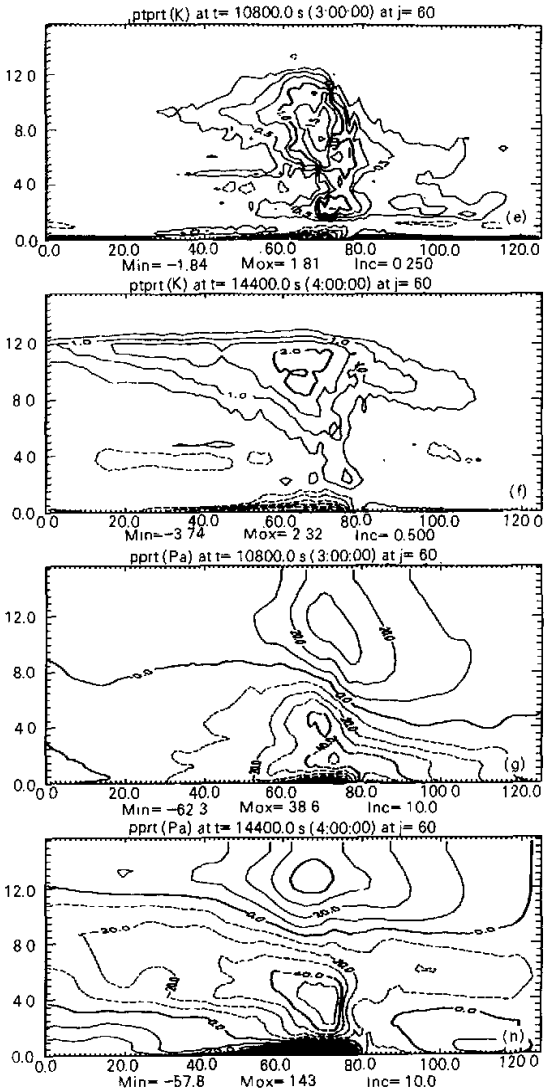

Fig. 3. Vertical cross-sections for 30-km line-averaged in experiment CRTL of the system-relative wind (1 m / s contour intervals) at (a) 3 h, (b) 4 h; vertical velocity (0.5 m / s contour intervals) at (c) 3 h, (d) 4 h; potential temperature perturbation at (e) 3 h(0.25 K contour intervals), (f) 4 h (0.5 contour intervals); pressure perturbation (10 hPa contour intervals) at (g) 3 h, (h) 4 h.

3.2.1 *System-relative-horizontal flow*

By 3 h into the simulation, the strong inflow ($u'<0$) is presented at 0–1 km height before leading line, and the maximum is situated near the low-level surface (Fig. 3a). The enhanced outflow ($u'<0$) appeared beneath the height of 1 km rearward leading line. At 1–4 km height rear of the leading line there is a distinct inflow ($u'>0$) region corresponding to the weak downdraft motion. Some part of this inflow coupled the low-level fore inflow to form the pronounced updraft near leading line in midlevel convergent region, simultaneously, other part of it coupled the rear outflow to form the low-level outflow jet. Another outflow flow region was situated above the 4 km height, which was associated with the upper-level stratiform cloud rear the leading line. Moreover, the pumping process resulted from the convergence of horizontal field due to the velocity trough situated in this height accelerated the low-level updraft and consequently formed the strong updraft.

The low-level fore inflow velocity increased in maximum from 14.2 ms^{-1} at 3 h to 18 ms^{-1} at 4 h (Fig. 3b). Subsequently, the rear midlevel inflow decreased in its extension, and inflow axis descended to 2 km height. Its maximum decreased from 5.15 ms^{-1} at 3 h to 2.68 ms^{-1} at 4 h. An upper-level flow jet appeared at 12 km height, which was associated with the upward transportation of momentum by the acceleration of updraft velocity.

3.2.2 *Vertical motion*

Fig. 3c shows the vertical motion in the vertical cross-section at $t=3$ h. Evidently the whole updraft region tilted with the height and spreading rearward. Two upward velocity maximums appeared at 4-km and 8-km height, respectively. The maximum vertical velocity is about 4.54 ms^{-1}. Supported by the warm and humid air in the boundary layer, the low-level strong updraft accelerated in convergence region. Hereafter it was affected by the upper-level divergent flow and the buoyancy associated to release latent heat from freezing water, a new updraft maximum appeared at 8-km height (Fig. 3d). Moreover, the upper-level updraft increased the growing of the stratiform cloud. These features could be interpreted as the consequence of the released latent heat by radiation cooling process and increased ice phase material. In addition, the low-level updraft region became narrower and updraft maximum increased simultaneously. Weak downdraft motion appeared beneath the updraft motion. Zipser (1969) and Brown (1979) suggested the mesoscale weak downdraft beneath the plume is associated with the evaporation cooling of precipitation in stratiform cloud. During this period, the updraft tilt of the convection system became more remarkable. Fig. 4 shows the vertical cross-section of the observed radar reflectivity (dBZ) and vertical velocity by Jorgensen et al. (1997). Comparison Fig. 3d with Fig. 4b reveals that the model could successfully simulate the vertical structure of vertical velocity of the squall line.

3.2.3 *Potential temperature perturbation*

Figs. 3e and 3f show the vertical cross-sections of the potential temperature perturbations at 3 h and 4 h, respectively. At $t=3$ h, a negative potential temperature anomaly was located at 0–1 km height rearward the squall line, which is generally named as the cold pool (Fig. 3e). The cold pool coincided with the oceanic surface precipitation and resulted from the evaporation of precipitation. Its intensity reaches its maximum immediately rear the leading line of squall line. The negative buoyancy due to the cold pool corresponding to the mesoscale downdraft has crucial impact on the evolution of the rearward tilt structure of the MCS (Weisman 1992, Trier et al., 1996). When the magnitude of the vertically integrated cool

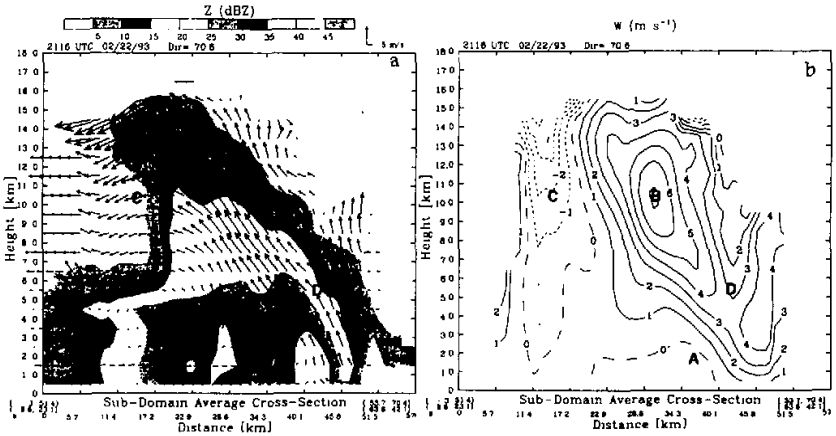

Fig. 4. Vertical cross-sections of (a) observation for Doppler radar reflectivity (dBZ) and vertical velocity (m / s) (after Jorgensen et al., 1997).

pool negative buoyancy exceeds the vertical shear of the ambient wind speed, the updraft tilt would be developed subsequently (Rotunno et al., 1988). In addition, a positive anomaly of potential temperature was situated above 1.5-km height that corresponded to the anvil cloud due to the warming of ambient by the latent heat released in freezing process in the upper troposphere. Moreover the positive anomaly of potential temperature extended lateral, and the anvil cloud appeared due to the upper-level divergent wind.

With the increasing of integrated time, the low-level cold pool increased in its intensity and extension, and the reward tilt of convective region became more distinct (Fig. 3f). Meanwhile the spatial extension of latent heat is increased, and the anvil cloud became more salient. Moreover, a narrow weak negative anomaly of potential temperature is located at 4 km height, i.e., the melting level far away from the leading line.

3.2.4 *Pressure perturbation*

The vertical cross section of the pressure perturbations at $t=3$ h and 4 h are shown in Figs. 3g and 3h, respectively. At $t=3$ hour, a meso-high ranged about 20 km in the horizontal and 0.5-km depth is located the rear of the leading edge that corresponding the low-level cold pool. The maximum intensity of mesohigh is about 38.6 hPa. Chin and Wilhelmson (1998) investigated a similar tropical squall line, and indicated that the cold mesohigh was associated with the subsidence flow. The forcing of the mesohigh could accelerate the adjacent segment of the squall line, and is the key reason for the squall line transition from linear stage to bow-shaped structure.

Moreover, a mesolow of 50 hPa maximum intensity situates from above the mesohigh noted earlier to about the height of 8 km, whose center situated beneath and immediately adjacent of the sloping updraft region. The mesolow is mainly related to the vertical gradient of buoyancy due to the condensation in updraft and evaporation in downdraft (Trier et al., 1996). Chin and Wilhelmson (1998) confirmed that a warm mesolow accompanied by the rear

mesohigh existed in front of the leading line of convection. At $t=4$ h, the low-level mesolow is increased in intensity and spatial extension that reached to 1-km height (Fig. 3h). However, the middle-level mesohigh elevated toward 4 km height, whereas the surface warm mesolow in front of the leading line decayed distinctly.

3.3 *Precipitation analysis*

The amount of the precipitation is an essential factor to assess the development of deep convection of MCS. The different precipitation types result from the different microphysics mechanism. The spatial distribution of precipitation varies from case to case. The asymmetrical warming resulted from the precipitation materials could feedback to the evolution and structure of convective system. In general, the precipitation of convective system cloud be classified to the frontal convective and rear stratiform cloud region. Of course, it is very difficult to distinguish two kinds of convection clearly.

Figs. 5a and 5b indicate the vertical cross-section of model-estimated radar reflectivity (dBZ) at $t=3$ h and 4 h, respectively. The dense-contoured region at the lower portion near the right side is corresponding to the maximum convective precipitation immediately behind the leading line. The maximum of dBZ is located about the 10 km rearward the leading edge of squall line at the surface (Fig. 5a). The contour of dBZ tilted with the height and varied with time (Fig. 5b). Comparison of the model-estimated radar reflectivity (Fig. 5b) with the actually observed counterpart (Fig. 4a) reveals that both of the vertical structures are very similar.

In the CRTL, the microphysical processes included the following three water phase categories: water vapor (q_v), cloud water (q_c), rain water (q_r), and three ice phases: cloud ice (q_i), snow (q_s), and hail (q_h). Figs. 6a and 6b show the vertical cross-section of the water vapor perturbation at 3 h and 4 h, respectively. In Fig. 6a, an narrow and positive water vapor anomaly situated at about the height of 1 km ahead of the leading line, corresponding to the strong front-to-rear inflow that carried moisture from the oceanic surface. Moreover, the slantwise updraft along with the moisture leads to another positive water vapor anomaly appeared at the 8-km height in the rearward tilt region. Below the positive anomaly, there is a negative water vapor anomaly resulted from evaporation of precipitation particles. With the increasing of integration time, there is an obvious positive correlation in the temporal tendency between the positive and negative anomaly (Fig. 6b). When the low-level convection increased, the more moisture was transported vertically and the positive anomaly aloft increased. In addition, the low-level negative anomaly is increased simultaneously since the rear precipitation is increased and more evaporation is induced. The vertical distribution of cloud water (q_c) primarily coincides with that of the positive water vapor anomaly, rangin g from 1 km to 10 km in the height (Fig. 6c). At $t=3$ hour, the two maxima of cloud water are located at 3-km and 6-km height, respectively. With the time increased, the vertical distribution of cloud water roughly remained its structure expect the rearward extension in the upper-level, where coincided with the stratiform cloud (Fig. 6d). However, the rainwater (q_r) was oriented uprightly and mostly present below the height of 4–5 km (just beneath the melting level). The maximum of rainwater primarily situated at rear of the strong updraft at the leading line (Fig. 6e). Comparison of the vertical distribution of model-estimated dBZ (Figs. 5a, b) with that of rain water (Figs. 6e and 6f) reveals that the large radar reflectivity at the low level results almost entirely from the contribution of rainfall. By 4 h, rainwater in the convective and stratiform cloud region is both increased, and the stratiform cloud region spreads its extension rearward (Fig. 6f).

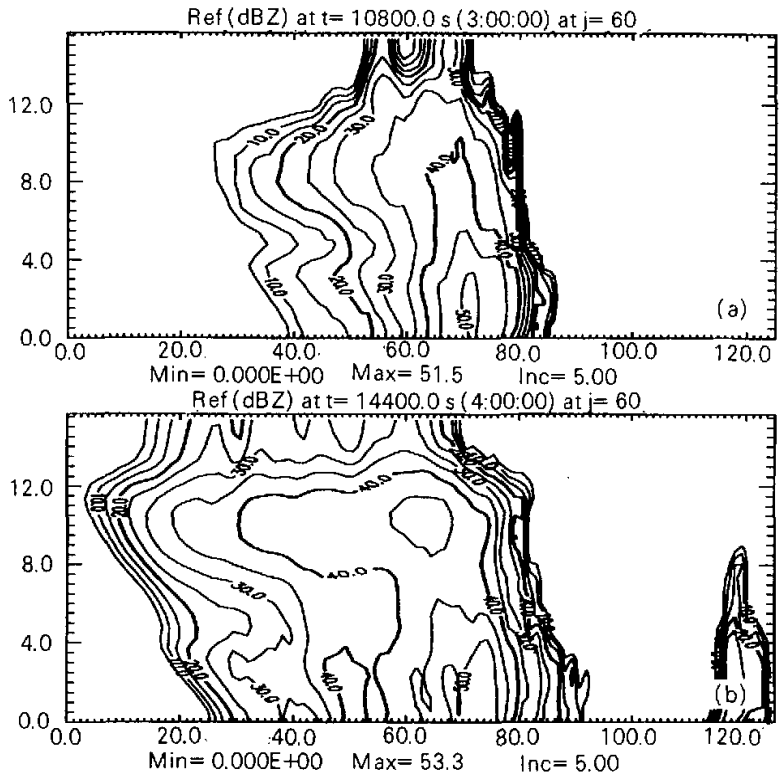

Fig. 5. Vertical cross-sections for the line-averaged model estimated radar reflectivity (dBZ) (5-dBZ contour intervals) at (a) 3 h, (b) 4 h.

Cloud ice (q_i) was mainly located in the stratiform cloud at upper-level ranging from 6 to 11 km height where the air temperature is relatively low, and the ice phase categories materials may be appeared. The stratiform cloud was not so distinct at 3h (Fig. 6g), however, the amount of cloud ice is increased, and the stratiform cloud extends rearward obviously at 4 h (Fig. 6h). Snow (q_s) is mostly located above the height of 6 km that shared the dominant part of all water categories in the upper stratiform cloud. The distribution of snow is relatively uniform, so that the amount in the convective and stratiform cloud is roughly equivalent (Fig. 6i). Of course, the total amount of snow (q_s) is slightly less than that of rainwater. By 4 h, the quantity of snow increased evidently and a narrow horizontal maximum appeared at about the height of 11 km (Fig. 6j). Such distribution pattern of snow is helpful to the release of latent heat and the development of anvil cloud in the upper troposphere. The hail (q_h) was mostly situated at mid- and upper-levels ranging from 3 to 10 km height (Fig. 6k). The maximum of hail was presented at 5-km height (melting level) rearward the convective region. The hail still existed below melting level till to 3 km, which associated with the convective intensity. The height of the hail formation is decreased in the case of weak convection. By 4 h, the region of hail expanded rearward almost reached twice of that at 3 h that resulted from the

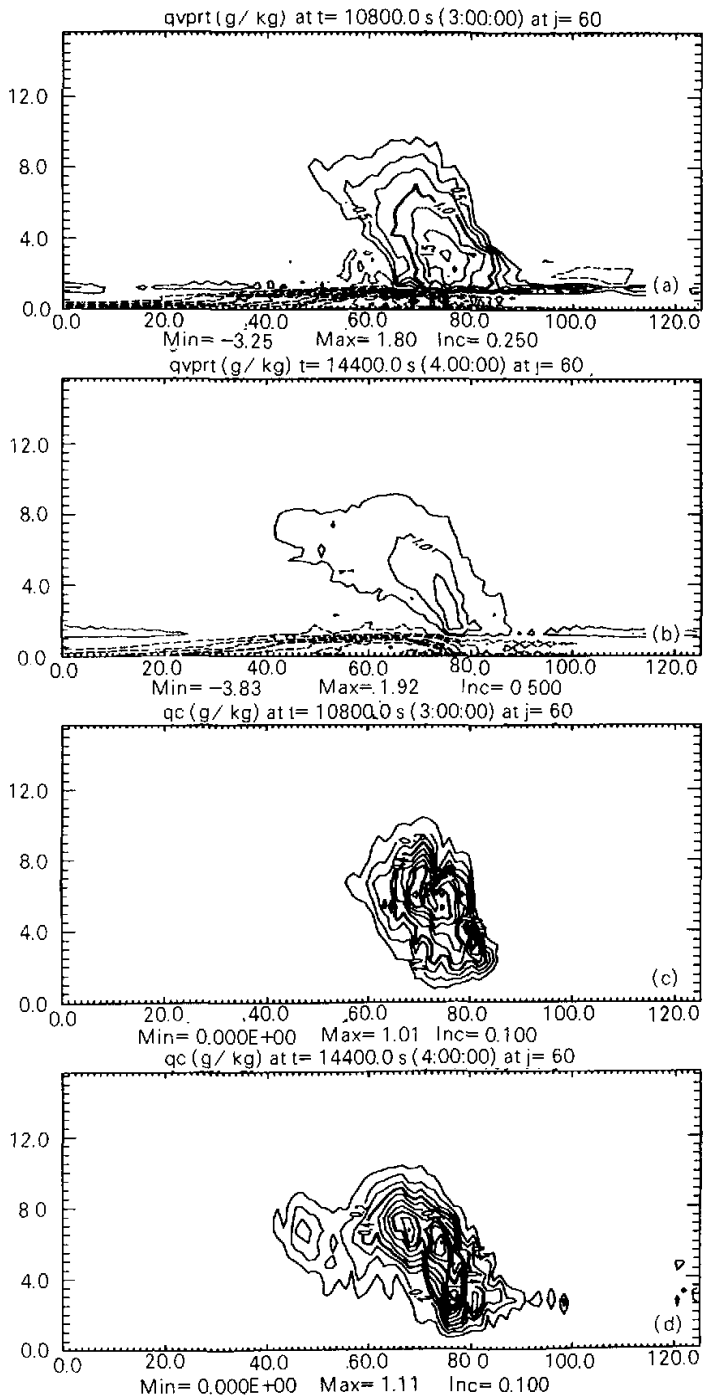
qvprt (g/ kg) at t= 10800.0 s (3:00:00) at j= 60
12.0
8.0
4.0
0.0
0.0
20.0
40.0
60.0
80.0
100.0
120.0
(a)
Min= −3.25 Max= 1.80 Inc= 0.250
qvprt (g/ kg) t= 14400.0 s (4:00:00) at j= 60
(b)
Min= −3.83 Max= 1.92 Inc= 0.500
qc (g/ kg) at t= 10800.0 s (3:00:00) at j= 60
(c)
Min= 0.000E+00 Max= 1.01 Inc= 0.100
qc (g/ kg) at t= 14400.0 s (4:00:00) at j= 60
(d)
Min= 0.000E+00 Max= 1.11 Inc= 0.100

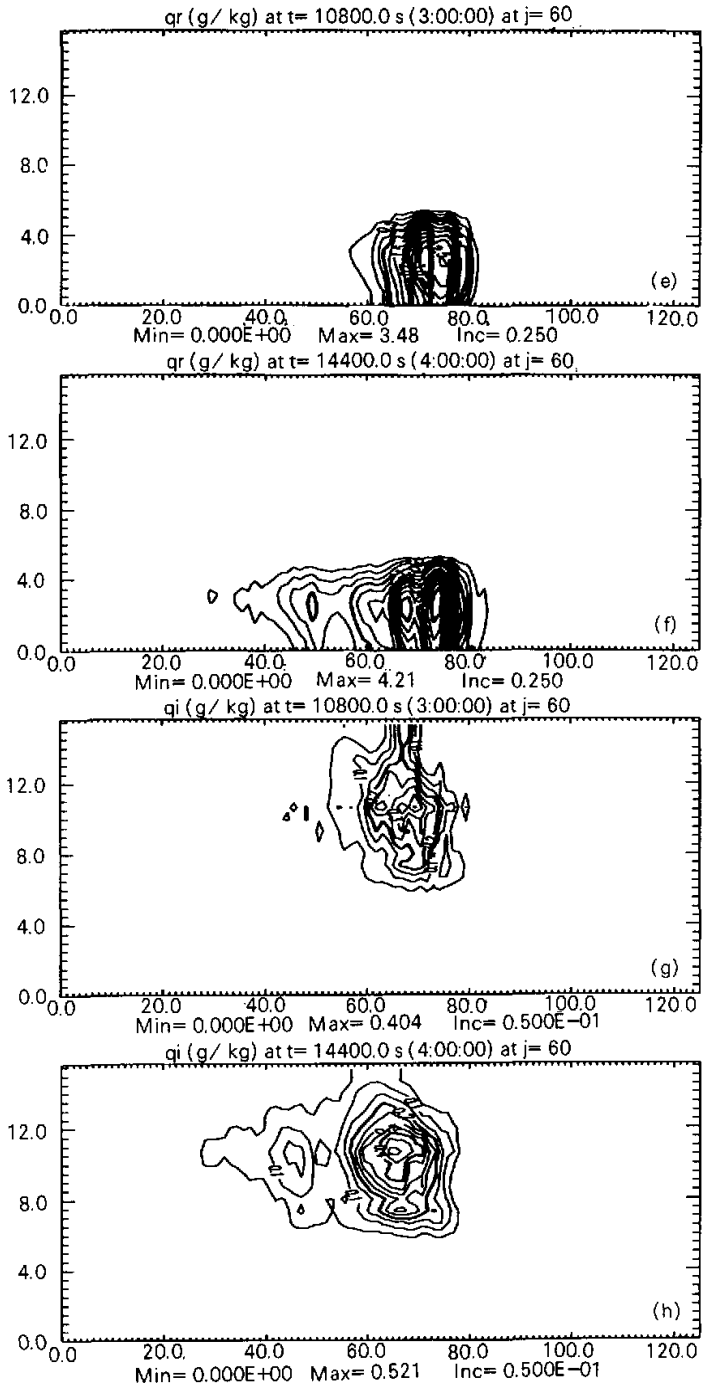
qr (g/ kg) at t= 10800.0 s (3:00:00) at j= 60
12.0
8.0
4.0
0.0
0.0
20.0
40.0
60.0
80.0
100.0
120.0
(e)
Min= 0.000E+00 Max= 3.48 Inc= 0.250
qr (g/ kg) at t= 14400.0 s (4:00:00) at j= 60
(f)
Min= 0.000E+00 Max= 4.21 Inc= 0.250
qi (g/ kg) at t= 10800.0 s (3:00:00) at j= 60
(g)
Min= 0.000E+00 Max= 0.404 Inc= 0.500E-01
qi (g/ kg) at t= 14400.0 s (4:00:00) at j= 60
(h)
Min= 0.000E+00 Max= 0.521 Inc= 0.500E-01

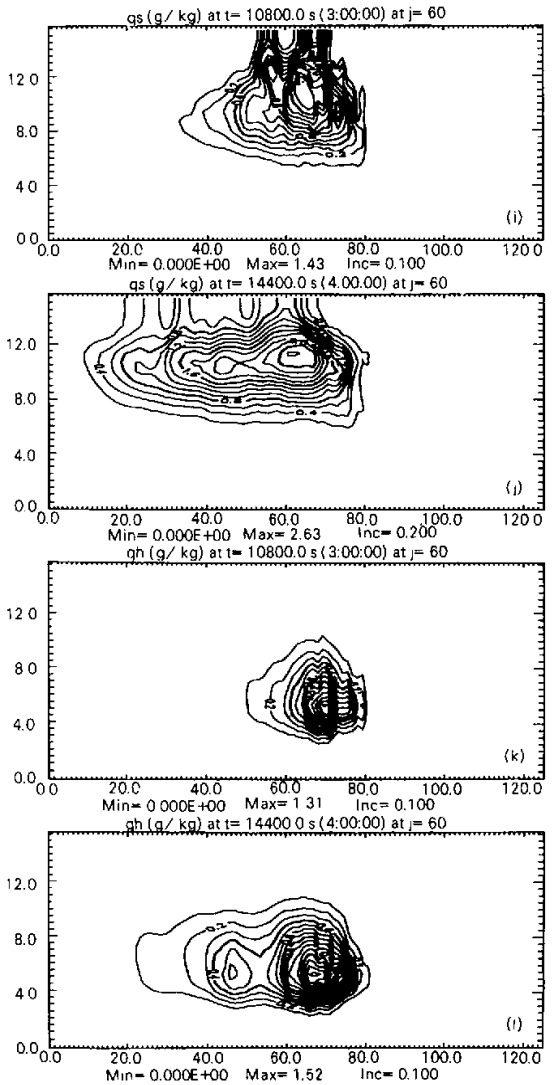

Fig. 6. Vertical cross-sections for the line average water vapor perturbation (0.25 g contour intervals) at (a) 3 h, (b) 4 h; cloud water (0.1 g / kg contour intervals) (c) 3 h; (d) 4 h; rain water (0.25 g / kg contour intervals) at (e) 3 h, (f) 4 h; ice (0.05 g / kg contour intervals) at (g) 3 h, (h) 4 h; snow at (i) 3 h (0.1 g / kg contour intervals), (j) 4 h (0.2 g / kg contour intervals); hail at (0.1 / kg contour intervals) (k) 3 h, (l) 4 h.

rearward development of the stratiform cloud (Fig. 6l).

4. Effect of different cloud microphysics process

In Section 3, we know that the initial development of convective system ranged from 0 h to 2 h, and the linear convective organization began to appear at about $t=2.5$ h. By 3 h, the relatively mature convective system already formed. In the forthcoming 1 hour, the convective system has been increasing in convection and precipitation intensity. The slantwise updraft structure and the rear vortexes generation are appeared at this time. In the this Section, the sensitive experiment in which Kessler warm rain microphysics processes were adopted will be investigated to assess the influence of cloud microphysics processes on the evolution of tropical squall line. In the Kessler warm rain processes, only three water phase categories, water vapor (q_v), cloud water (q_c) and rainwater (q_r) are included.

Fig. 7 represents time–history of the maximum updraft, maximum downdraft and the

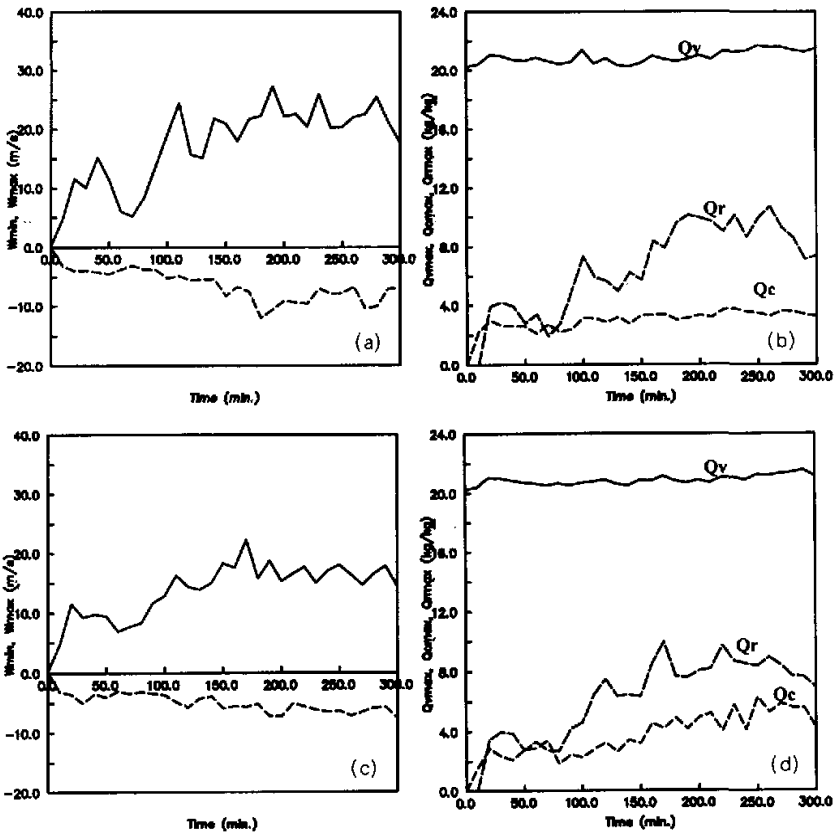

Fig. 7. Evolution for maximum and minimum value of model's variable in the experiment CTRL (a) vertical veocity (b) water vapor (Q_v), rain water (Q_r), cloud (Q_c); and in the experiment WARM (c) vertical velocity, (d) water vapor (Q_v), rain water (Q_r), cloud (Q_c).

quantities of water categories in CTRL and WARM experiments. Comparison of Fig. 7a with 7c reveals that there were little differences between WARM and CTRL for the vertical velocity in the initial adjustment process of convection. However, the maximal magnitudes of updraft or downdraft in WARM were less than that in CTRL with the time increasing. Comparison of Fig. 7b with 7d shows that the time of maximal rainfall appeared in WARM is earlier than that in CTRL. Moreover, the maximums of rainfall in WARM were less than that in CTRL from then on. When the time exceeded 150 minutes, the cloud water in WARM was relatively more than that in CTRL due to the more stratiform cloud developing in WARM.

Figs. 8a and 8b show the low-level horizontal wind and vertical velocity fields at 3 h and 4 h in WARM, respectively. By 3 h, the squall line had evolved from linear stage to bow-shaped structure (Fig. 8a). Evidently, the bow-shaped structure reached its extent more than that in the CTRL. In addition, the bow-shaped structure is still kept at 4 h (Fig. 8b). Subsequently, the squall line begins to break into pieces due to the relatively slow movement of northern segment contrasted with accelerative motion of southern portion.

Comparison of Fig. 8 with Figs. 2a, 2c reveals that the convection was relatively weak and increased slowly in WARM comparison with that in CRTL. In addition, the whole life period of convective system is relatively short accompanied by more bow-shaped structure and earlier appearing of strong convection in WARM. In the updraft motion the conflicts between the positive thermal buoyancy resulted from the condensation process and the negative counterpart due to water loading could affect further development of convection. In the upper troposphere, the active ice phase processes could produce more latent heat due to rather low ambient temperature. Hence the positive buoyancy resulted from freezing process exceeds the negative buoyancy resulted from water load. Cotton and Anthes (1989) suggested that restricting of the warm rain processes might benefit to the development of the convection. Therefore, the generation and maintenance of deep convection was more easily in CTRL. In contrast, the convection in WARM is weak and the convective system could only sustained for a short time due to the less energy releases from the condensation process. In addition, the air parcel in the weak updraft could stay a relative longer time and mix and / or entertain with ambient cold dry air easily that eliminates the rapid development of convection in some degree.

Fig. 9a shows the vertical cross-section of vertical velocity at $t=4$ h in WARM. Comparison of Fig. 9a with Fig. 3d reveals that the two maximums of vertical velocity at low- and upper-level still sustained in WARM. However, the convective system had a larger extension of updraft and downdraft, but less intensity than that in CTRL. In addition, the updraft region at the upper-level in WARM was obviously larger and the rearward tilt structure became more pronounced than ever.

Fig. 9b shows that a negative potential temperature anomaly was situated at 12-km height and resembled a cold hat covered the top of the cloud. However, no such structure appeared in CTRL. Since in WARM the ice phase processes were excluded and the warming of ambient by latent heat released from freezing water categories never happened, so the negative potential temperature anomaly appeared only at the upper-level. The cold-hat structure could add an negative buoyancy in the convection and inhibits the development of convection at the upper troposphere.

The vertical cross-sections of cloud water and rainwater at 3 h in WARM are shown in Figs. 9c and 9d, respectively. The upright extent of cloud water and rainwater in WARM were evidently larger than that in CTRL (Figs. 6c, 6e). In WARM the cloud water region upward reached about the height of 12 km (Fig. 9c). With the increasing of time, the horizontal

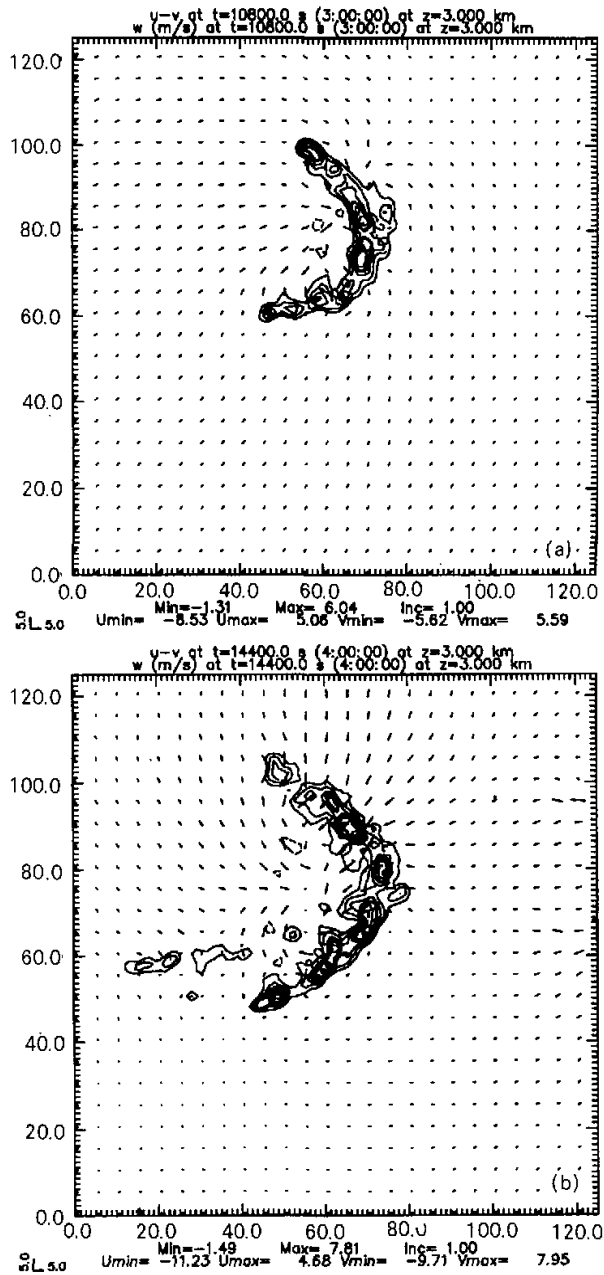

Fig. 8. Vertical velocity at 3 km MSL in intervals of 1 m/s (positive values solid, negative values dashed) and system-relative wind vectors at 3 km MSL for the experiment WARM at (a) 3 h, (b) 4 h.

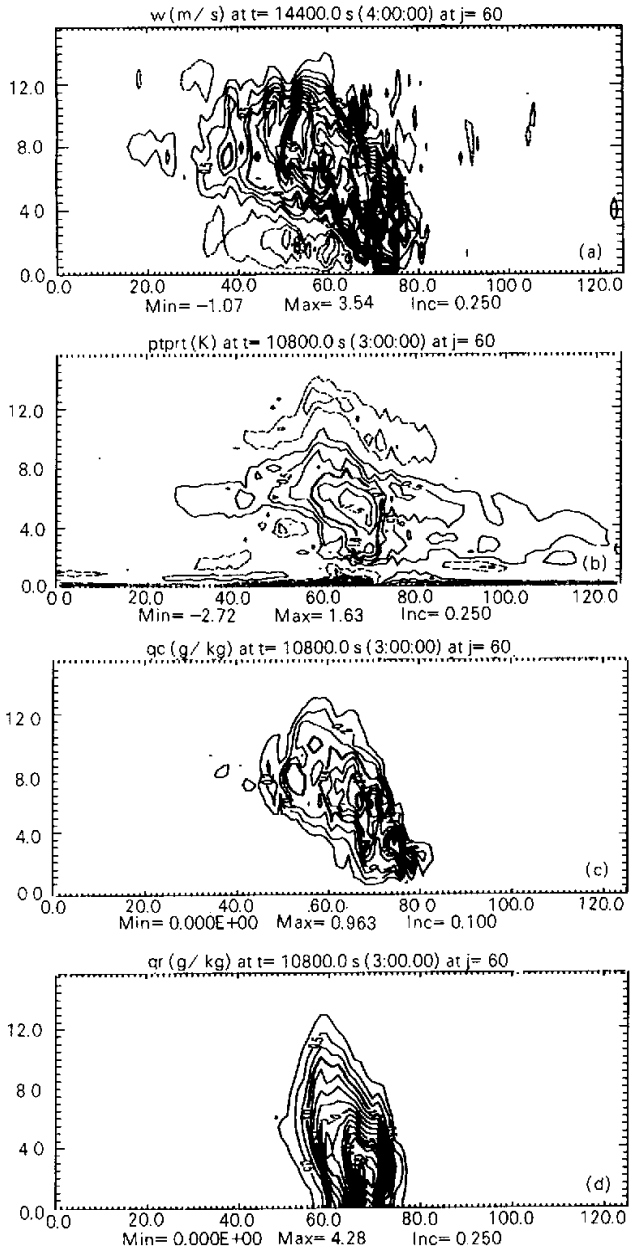

Fig. 9. Vertical cross-sections for 30-km line-averaged in experiment WARM of (a) vertical velocity (0.25 m / s contour intervals) at 4 h, (b) perturbation potential temperature (0.25 K contour intervals) at 3 h; (c) cloud water (0.1 g / kg contour intervals) at 3 h; (d) rain water (0.25 g / kg contour intervals) at 3 h.

extension of cloud water became larger and reached almost twice of that in CTRL. Fig. 9d reveals that in early stage of WARM the rainwater extended its vertical range towards 12km height, whereas in CTRL this just located the 4 km height, and the rainfall intensity is larger than that in CTRL. In the latter stages, the horizontal extent of rainwater was larger than that in CTRL, but its maximum was less than that in CTRL (figure omitted). When the ice phases were included, the suspension of hail particles in updrafts at the upper troposphere would delay the surface precipitation. Whereas in WARM the ice phase processes at the upper level are replaced by the condensation process, the region where rain particles formed upward approached to the height of 12 km and the quantity of rain particles increased. So contrasted to CTRL, the increased liquid–phased rainfall would induce the excessive evaporation of subcloud water load in the early stage of the squall line in WARM. The evaporation cooling would result in the relative stronger subcloud downdraft, cold pool and more rearward updraft tilt consequently (Fig. 9a).

From the above analysis, we could conclude that ice phase materials have pronounced impacts on the convective system. The following effects of cloud microphysical processes will be available on the evolution of squall line. Since the additional positive buoyancy resulting from the latent heat released in the freezing process exceeds the negative buoyancy produced by the water loading, the development of deep convection could be enhanced and long lively maintained. The ice phase particles that falling at relatively rapid speed would influence the occurrence time of precipitation and redistribute the water loading, for instance, shifted surface precipitation or heavy rainfall to an earlier time. Moreover, the rainfall within the downdraft region provides a source of evaporation, and redistributes the quantity of all categories of water. Consequently, the inside circulation of the convective system was changed.

5. Conclusions

In this paper, the ARPS model is performed to simulate the squall line occurred on 22 February 1993 over the equatorial Pacific Ocean. The influences of different cloud microphysical processes on the structure and evolution of the squall line were investigated by the sensitive experiment. The simulation results reveal that the cloud–resolving ARPS model could successfully simulate three–dimensional dynamic, thermodynamic structure and evolution of the tropical squall line. In the sensitive experiments in which different cloud microphysical processes were adopted are conducted. Comparison between CTRL and WARM reveals that more latent heat released in ice phase microphysical processes would benefit to the development of deep convection and the convective system could sustain for a longer time. Whereas the convection in warm rain processes was relatively weak and the squall line develops rapidly in its early stage, which resulted in earlier transition from linear stage to the bow–shaped structure. Moreover, the ice phase processes are available for the growth of convective region, whereas warm rain processes are in favor of the development of rear stratiform cloud.

Although the ARPS model could simulate the tropical squall line rather well in this study, the linear draft structure appeared slowly and convective organization behaved itself as some discrete convective cells at the earlier stage (0–2 h) of this simulation. This phenomenon is partly associated with the cold start problem of the model, and may be a reason why the simulated convection development comparatively slower than actual observations. In addition, how the mesoscale systems influence large–scale circulation? What are the statistical features of dynamics and thermodynamics in modeled region, and the large–scale effect on

convective system needs to be farther investigated.

The authors thank to Mr. Fei Shiqiang and Zhang Jin who provided many helpful supports in this research work. The simulations were made using the Advanced Regional Prediction System (ARPS) developed by the Center for Analysis and Prediction of Storms (CAPS), University of Oklahoma. CAPS is supported by the National Natural Science Foundation and the Federal Aviation Administration through combined grant ATM92-20009.

REFERENCES

Brown, J. M., 1979: Mesoscale downdrafts driven by rainfall evaporation: a numerical study. *J. Atmos. Sci.*, **36**, 313-338.

Chin, H.-N., and R. B. Wilhelmson, 1998: Evolution and structure of squall line elements within a moderate CAPE and strong low-level jet environment. *J. Atmos. Sci.*, **55**, 3089-3113.

Cotton, W. R. and R. A. Anthes, 1989: *Storm and cloud dynamics*. Academic Press, Inc. 883pp.

Ferrier, B. S., W.-K. Tao, and J. Simpson, 1995: A double moment multiple-phase four-class bulk ice scheme. Part II: Simulations of convective storms in different large-scale environments and comparisons with other bulk parameterizations. *J. Atmos. Sci.*, **52**, 1001-1033.

Houze, R. A., 1982: Cloud clusters and large-scale vertical motions in the tropics. *J. Meteor. Soc. Japan*, **60**, 396-410.

Jorgensen, D. P., M. A. LeMone, and S. B. Trier, 1997: Structure and evolution of the 22 February 1993 TOGA COARE squall line: aircraft observations of precipitation, circulation, and surface energy fluxes. *J. Atmos. Sci.*, **54**, 1961-1985.

Moncrieff, M. W., S. K. Krueger, D. Gregory, J.-L. Redelsperger, and W.-K. Tao, 1997: GEWEX Cloud System Study (GCSS) Working Group 4: Precipitating convective cloud systems. *Bull. Amer. Meteor.*, **78**, 831-845.

Redelsperger, J. L., P. R. A. Brown, F. Guichard, C. Hoff, M. Kawasima, S. Lang, T. Montmerle, K. Z. Nakamura, K. Saito, C. Seman, W. K. Tao and L. J. Donner, 2000: A GCSS model intercomparison for a tropical squall line observed during TOGA-COARE, Part I: Cloud-resolving models. *Quart. J. R. Meteor. Soc.*, **126**, 823-864.

Rickenbach, T. M., and S. A. Rutledge, 1998: Convection in TOGA COARE: Horizontal scale, morphology, and rainfall production. *J. Atmos. Sci.*, **55**, 2715-2729.

Rotunno, R., J. B. Klemp, and M. L. Weisman, 1988: A theory for strong long-lived squall lines. *J. Atmos. Sci.*, **45**, 463-484.

Tao, W.-K., and J. Simpson, 1989: Modeling study of a tropocal squall-type convective line. *J. Atmos. Sci.*, **46**, 177-202.

Trier, S. B., W. C. Skamarock, M. A. LeMone, and D. B. Parsons, 1996: Structure and evolution of the 22 February 1993 TOGA COARE squall line: numerical simulations. *J. Atmos. Sci.*, **53**, 2861-1886.

Trier, S. B.,W. C. Skamarock and M. A., LeMone, 1997: Structure and evolution of the 22 February 1993 TOGA COARE squall line: organization mechanisms inferred from numerical simulation. *J. Atmos. Sci.*, **54**, 386-407.

Webster, P. J. and R. Lukas, 1992: TOGA COARE: The Coupled Ocean-Atmosphere Response Experiment. *Bull. Amer. Meteor. Soc.*, **73**, 1377-1416.

Weisman, M. L.,1992: The role of convectively generated rear-in-flow jets in the evolution of long-lived mesoconvective systems. *J. Atmos. Sci.*, **49**, 1827-1847.

Xue, M., K. K. Droegemeier, V. Wong, A. Shapiro, and K. Brewster, 1995: Advanced Regional Predication System (ARPS) Version 4.0 User's Guide, Center for Analysis and Prediction of Storms (CAPS), Univ. of Oklahoma, U.S.A. 320pp.

Zipser, E. J., 1969: The role of organized unsaturated convective downdrafts in structure and rapid decay of an equatorial disturbance. *J. Appl. Meteor.* **8**, 799-814.

热带飑线结构和演变的数值模拟研究 第一部分: 云分辨模式

孙廷凯 谈哲敏

摘 要

利用风暴尺度、云分辨的数值模式 ARPS 模拟了 1993 年 2 月 22 日 TOGACOARE 试验期间在赤道南太平洋观测到一次热带海洋飑线过程的发生发展过程, 验证该模式的模拟热带对流系统的能力, 并详细地分析了该次飑线的结构特征和动力学形成机制。通过数值敏感性试验研究了不同的云微物理过程对热带飑线的结构和发展演变过程的影响, 所考虑的云微物理过程分为包含六种水相态的冰相过程和 Kessler 暖雨过程。模拟结果表明, 云分辨模式 ARPS 采用合适的物理过程可以较成功地模拟出热带飑线的三维结构及其演变过程。数值敏感性试验结果表明, 在对流上升过程中, 由于与冻结作用有关的冰相微物理过程能释放更多的潜热, 这种潜热能产生垂直方向上的浮力梯度从而较明显地加强系统的深对流, 有利于对流系统组织性的对流带的长时间维持; 相比之下, 暖雨过程中飑线的生命周期缩短, 而系统倾斜结构更明显, 层状云区的发展比较旺盛。

关键词: 飑线, 冷池, 冰相微物理, 云分辨模式